Dear author,

Please note that changes made in the online proofing system will be added to the article before publication but are not reflected in this PDF.

We also ask that this file not be used for submitting corrections.

Cement and Concrete Research xxx (2015) xxx–xxx

Contents lists available at ScienceDirect

Cement and Concrete Research

journal homepage: www.elsevier.com/locate/cemconres

A study on the corrosion of reinforcing bars in alkali-activated fly ash mortars under wet and dry exposures to chloride solutions

C. Monticelli [a,*], M.E. Natali [b], A. Balbo [c], C. Chiavari [d,e], F. Zanotto [f], S. Manzi [g], M.C. Bignozzi [h]

[a] Centro di Studi sulla Corrosione e Metallurgia "A. Daccò", Università di Ferrara, Via Saragat 4a, 44122 Ferrara, Italy
[b] Dipartimento di Ingegneria Civile, Chimica, Ambientale e dei Materiali, Università di Bologna, Via Terracini 28, 40131 Bologna, Italy
[c] Centro di Studi sulla Corrosione e Metallurgia "A. Daccò", Università di Ferrara, Via Saragat 4a, 44122 Ferrara, Italy
[d] C.I.R.I. (Centro Interdipartimentale Ricerca Industriale) Meccanica Avanzata e Materiali, Università di Bologna, Bologna, Via Terracini 28, 40131 Bologna, Italy
[e] Dipartimento di Beni Culturali, Università di Bologna, Via degli Ariani, 1, 48121 Ravenna, Italy
[f] Terra&Acqua Tech, Università di Ferrara, Via Saragat 4a, 44122 Ferrara, Italy
[g] Dipartimento di Ingegneria Civile, Chimica, Ambientale e dei Materiali, Università di Bologna, Via Terracini 28, 40131 Bologna, Italy
[h] Dipartimento di Ingegneria Civile, Chimica, Ambientale e dei Materiali, Università di Bologna, Via Terracini 28, 40131 Bologna, Italy

ARTICLE INFO

Article history:
Received 6 February 2016
Received in revised form 24 May 2016
Accepted 27 May 2016
Available online xxxx

Keywords:
D. Alkali activated cement
C. Corrosion
D. Chloride
C. Mechanical properties
B. Microstructure

ABSTRACT

This research investigates the corrosion protection afforded to the embedded rebars by room temperature-cured alkali-activated mortars, based on class F fly ash (FA), during wet and dry (w/d) exposures to 0.1 M NaCl solution. The results were compared to those obtained in a traditional cement-based mortar (REF). The rebar corrosion behaviour was characterized by corrosion potentials (E_{cor}) and potentiostatic polarization resistance (R_p) measurements, polarization curve recording and electrochemical impedance spectroscopy (EIS). The information collected suggested that FA mortars afforded a lower corrosion protection to the rebars and the reason was investigated by microstructural, physical–mechanical and chemical analyses of the mortars. FA mortars were found to undergo a fast carbonation, so that depassivation of the rebars occurred concurrently, in spite of a limited total chloride content inside these mortars. REF mortar was much less susceptible to carbonation and rebar corrosion started when a sufficiently high chloride concentration was built up.

1. Introduction

The increasing focus on issues concerning environmental sustainability and the enhancement of recycled materials and industrial wastes is stimulating research into the development of alternative sustainable building materials. With regard to traditional construction materials, the environmental impact of ordinary Portland cement (OPC), which produces nearly one ton of CO_2 per ton of cement, is well-known. 50% of its carbon dioxide emissions are caused by the processing of raw materials, 40% by the fuel consumption required to achieve the high processing temperatures (1450 °C) and the remaining 10% by the use of electricity and transportation [1]. Similar considerations may also apply to traditional ceramic materials (bricks and tiles), for which natural origin raw materials and high processing temperatures are used (between 1000 and 1300 °C).

Alkali-activated materials (AAMs), which include geopolymers as the subset with the higher amount of silica and alumina and the lowest content of calcium oxide, represent a viable alternative to traditional building materials [2,3]. The alkali activation is a chemical process, which induces dissolution/reprecipitation reactions on amorphous alumino-silicate powders giving origins to solid products quite similar to cement paste or ceramics. The consolidation process takes place at moderate temperatures (20 ≤ T ≤ 100 °C) and, thanks to their specific chemical compositions, it is possible to activate various types of industrial wastes such as ground-granulated blast furnace slag (GGBS), coal-derived fly ash (FA) and other types of precursors derived from waste streams such as coal gangue and red mud [4]. These kinds of wastes are today only partially used, and without large opportunities for recycling, so that they are commonly disposed in landfills. The sustainability advantage of the alkali activation process is thus evident, as it allows the realization of materials that can be used as alternatives to OPC pastes or ceramics, with the same forming techniques (casting, extrusion, etc.) and final performances.

In view of exploiting the potentialities of AAMs as construction materials, the scientific community is now concentrated in understanding and optimizing the geopolymerization process and much work is focused on achieving high material durability [5–7]. Concerning

* Corresponding author.
E-mail addresses: mtc@unife.it (C. Monticelli), mariaelia.natali2@unibo.it (M.E. Natali), andrea.balbo@unife.it (A. Balbo), cristina.chiavari@unibo.it (C. Chiavari), federica.zanotto@unife.it (F. Zanotto), stefania.manzi4@unibo.it (S. Manzi), maria.bignozzi@unibo.it (M.C. Bignozzi).

http://dx.doi.org/10.1016/j.cemconres.2016.05.010
0008-8846/

reinforced structures, it is very important to understand if alkali-activated binders can guarantee the steel reinforcements a protectiveness comparable to that offered by OPC, also in aggressive environments. In fact, corrosion of reinforced elements is one of the main causes of structural failures, generally connected to carbonation and/or chloride penetration [8].

The corrosion behaviour of steel rebars in activated fly ash mortars depends on many factors, which still need to be fully investigated. Among these factors, the composition and nature of alkaline activator, the mortar/concrete curing temperature and the exposure conditions play a fundamental role. As far as the activating solution composition is concerned, it was found that the addition of sodium silicate to sodium hydroxide stimulated network formation in geopolymers so leading to improved mechanical strength, lowering chloride ion mobility and slightly improving corrosion performances [9–11]. However, also a high sodium hydroxide content was observed to improve the geopolymer protective properties because of stimulation of the geopolymerization rate [12]. The addition of an alkaline solid activator based on sodium silicate and sodium carbonate induced a descending alkaline pH in mortar specimens and/or a high total porosity [13]. In geopolymers, the presence of high concentrations of inhibiting silicate ions in the pore electrolyte was reputed to contribute to reinforce steel passivity [14,15]. The durability of reinforced geopolymer specimens in high relative humidity atmosphere was proved to be quite high and comparable to that in traditional mortars, in the absence of admixed chlorides or in the presence of a limited chloride contamination. Instead, the addition of 2% chlorides to the mortar mixes impaired the stability of the rebar passive films [10,13,16]. During continuous contact with 3.5% NaCl solution [10] or wet and dry (w/d) exposure to this solution [12], the performances of reinforced geopolymer specimens were slightly better than those in OPC-based reference specimens. The latter alternated immersion tests were carried out on high temperature-cured geopolymer specimens to improve the concrete performances. Actually, high temperature curing is a quite common way to achieve high geopolymer durability [9,12,13,16,17], although this reduces the material environmental sustainability and its use on building sites. Thus, many efforts aim at formulating room temperature (RT) activation of these new construction materials [18–21].

The aim of this paper was to evaluate the performances of reinforced RT-cured geopolymer mortars subjected to w/d cycles in chloride solution. Three different mortar compositions were formulated by modifying the Na_2O/SiO_2 ratio and their performances were compared to those of a traditional cement-based mortar. The corrosion behaviour of the embedded rebars was investigated by electrochemical tests (potentiostatic polarization resistance (R_p) measurements, electrochemical impedance spectroscopy (EIS) and polarization curve recording) and by a concomitant physical–chemical investigation of the mortar microstructures and characteristics, which helped interpretation of electrochemical test results.

2. Materials and methods

2.1. Raw materials

Geopolymers were prepared using class F FA sourced from the Enel Produzione S.p.A Italian power station of Torrevaldaliga, Civitavecchia, Roma and supplied by General Admixtures S.p.A. (Ponzano Veneto, Treviso, Italy). It is a fine (d_{50} = 22 μm) and mostly amorphous FA (65 ± 0.8 wt.%) with chemical composition, expressed in main oxide content, as follows: SiO_2 = 49.0, Al_2O_3 = 29.2, Fe_2O_3 = 2.7, CaO = 6.6, MgO = 1.1, SO_3 = 0.3, Na_2O < 0.05, K_2O = 0.6 wt.%. A detailed characterization of this FA is reported elsewhere [20].

The chosen activator solutions for the studied systems consisted in different mixtures of sodium silicate solution (SiO_2/Na_2O = 1.99 as molar ratio, density at 20 °C = 1.5 ± 0.2 g/cm^3, Ingessil, Verona, Italy) and 8 M NaOH solution, which were pre-mixed 24 h before sample preparation and additionally stirred immediately before casting.

CEM II/A-LL 42.5 R was used as reference binder while natural sand with standardized grain size distribution according to EN 196-1 [22] was used as aggregate for FA and cement-based mortar samples.

2.2. Mortar design and characterization

The samples were prepared by keeping constant both the binder amount (FA or cement) and the binder/sand and liquid/binder (L/B) ratios (binder/sand = 1:2.7 and L/B = 0.52). For geopolymers, the liquid part consisted in a fixed amount of alkaline solutions (10.7 wt.%) plus water (1.6 wt.%). Three different mixes of geopolymers were prepared by changing the relative amounts of 8 M NaOH and sodium silicate solutions in order to achieve specific molar ratios of Na_2O/SiO_2, namely equal to 0.12, 0.14 and 0.16 (chosen on the basis of previous works [10,20]). Geopolymer mortars were referred to as G_1, G_2 and G_3 (Na_2O/SiO_2 = 0.12, 0.14 and 0.16, respectively), while cement mortar samples were named REF.

Before casting, the mortar consistency was determined in the fresh state by flow-table test. All the slurries exhibited a good consistency showing an average spread diameter of about 200 mm. Geopolymer slurries were denser compared to REF and, among the FA-based formulations, G_3 exhibited the fastest setting time (20 min compared to 40 min, as average) thus meaning that the presence of a higher content of NaOH accelerates consolidation reactions.

The slurries were cast in different types of moulds (cylinders, prisms or cubes), depending on the characterization tests.

Sixteen cylinders (h = 100 mm, φ = 35 mm) were cast for each type of mortar. Ten cylinders were prepared for electrochemical tests with embedded rebars (acting as working electrodes, W) and activated titanium wires (acting as quasi-reference low-impedance electrodes (R)), which were fixed in the proximity of each reinforcement (Fig. 1a).

The rebars were ribbed carbon steel rods (sandblasted surface, φ = 10 mm) with both ends masked by epoxy paint. This surface protection was made more long-lasting by applying a further thermoset band on the paint. The area of the exposed surface was 1000 mm^2. These rebars were positioned along the longitudinal axis of the cylindrical samples, so that the mortar cover was about 13 mm.

Further six unreinforced cylinders were prepared for chloride content and pH measurements (Fig. 1b).

Prismatic samples (40 × 40 × 160 mm^3) and cubes (100 × 100 × 100 mm^3) were also cast, for mechanical and microstructural characterization and chloride diffusion test, respectively.

Both geopolymer and REF mortar samples were vibrated on a shaker table to reduce entrained air and cured for 28 days under conditions chosen with the aim to maximize their mechanical properties. In particular, independently from the absence or presence of a reinforcing bar, geopolymers were cured at T = 25 °C and R.H. = 35%, while REF samples were cured at T = 25 °C and R.H. > 95% until testing.

After 28 days of curing, epoxy varnish was applied to screen all reinforced cylinder surfaces, with the exception of the surface surrounding the exposed rebar region (Fig. 1a). The same screening geometry was adopted for unreinforced samples (Fig. 1b) to produce similar chloride penetration paths.

After the same curing time, physical–mechanical properties such as bulk density, compressive strength, dynamic elastic modulus and mortar shrinkage were investigated. In particular, bulk density (ρ in g/cm^3) was determined from mass/apparent volume ratio. Compressive strengths (σ_c) were measured by an Amsler–Wolpert machine (maximum load: 100 kN) at a constant displacement rate of 50 mm/min. The results are reported as average values of 5 measurements. Dynamic elastic modulus (E_d) was calculated as an average of 3 measurements, according to the formula $E_d = \rho \cdot V^2$, where V is the ultrasonic pulse

Please cite this article as: C. Monticelli, et al., A study on the corrosion of reinforcing bars in alkali-activated fly ash mortars under wet and dry exposures to chloride solutions, Cem. Concr. Res. (2015), http://dx.doi.org/10.1016/j.cemconres.2016.05.010

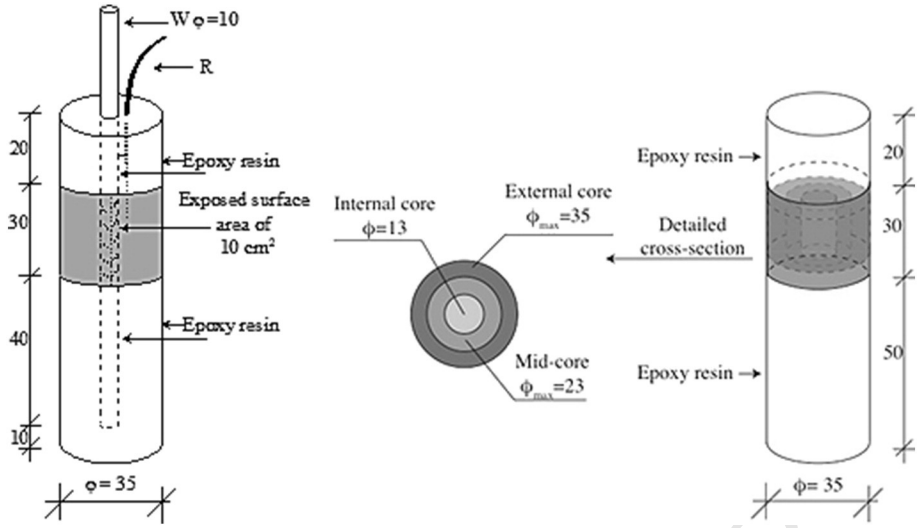

Fig. 1. Geometric framework of the cylinders (dimensions are expressed in mm): a) reinforced cylinder: W = working electrode, R = activated Ti reference electrode; b) unreinforced cylinder with detailed cross-section for Cl-analysis.

velocity, measured by a Matest instrument with 55 kHz transducers. The mortar shrinkage was determined according to EN 12617-4 [23].

The mortar microstructure, in terms of pore size distribution, was studied by a mercury intrusion porosimetry (MIP) (Carlo Erba 2000) equipped by a macropore unit (Model 120, Fison Instruments). A mercury surface tension of 0.48 N/m and a contact angle of 141.3° were assumed [24].

Mortar cubes were prepared according to ASTM C1556 [25], in order to evaluate chloride diffusion coefficients, which depend on total volume, dimensions and tortuosity of the mortar pores. After 28 days of curing, the cube surfaces were dried and sealed according to the standard method. Then, they were saturated in calcium hydroxide (REF) or sodium hydroxide solutions (geopolymers), before exposure to 165 g/l NaCl for 38 days. The chloride concentrations at eight recommended depth intervals were determined on powdered mortar samples according to ASTM C1152/C1152M [26] and ASTM C114 [27], while apparent chloride diffusion coefficients (D_a, m^2/s) were calculated by fitting the chloride profiles to the error-function solution to Fick's second law.

2.3. Exposure conditions

Reinforced and unreinforced cylindrical samples were exposed to 11 weekly w/d cycles. Each cycle consisted in 4 days of immersion in 0.1 M NaCl solution and 3 days of drying under laboratory conditions (T = 21 °C, R.H. = 35%). The NaCl solution was periodically refilled by distilled water and renewed each two cycles to avoid any possible change of concentration.

2.4. pH and chloride content measurements

At intervals, during the exposure, unreinforced cylinders were cut and drilled to obtain three coaxial cores, with different maximum diameter, Φ_{max}, (Fig. 1b).

After 2 and 11 w/d cycles, mortar portions coming from the innermost mortar cores were ground for pH measurements. In particular, 5 g of these mortar specimens was mixed with 5 cm^3 distilled water at RT and the pH of the obtained leachate solution was deemed to be an acceptable approximation of the pH of the mortar pore electrolyte [11,28]. Each pH value was the average of three measurements. Reference pH values were collected just after 28 days of curing. Geopolymer specimens for pH control were cured in plastic bags to avoid any pH drift due to carbonation.

After 2, 4, 6, 8 and 11 w/d cycles, the total chloride concentrations were also measured in all three coaxial cores obtained from each unreinforced cylinder, according to standard methods [26,27].

2.5. Electrochemical tests

2.5.1. Potentiostatic R_p measurements

Electrochemical tests were performed on reinforced cylindrical samples exposed to w/d cycles. Corrosion potential (E_{cor}) and potentiostatic polarization resistance (R_p) measurements were obtained by a 273A PAR instrument, mainly during the wet step of the cycles. E_{cor} values were measured both versus the inner Ti quasi-reference electrode and versus an external saturated calomel electrode (SCE), placed beside the mortar surface close to the bare rebar surface. During potentiostatic tests, a coaxial stainless steel net was positioned around the cylinders and acted as a counter electrode. For measurements carried out in the dry stage of the cycles, the external stainless steel net was secured around the mortar cylinder with an interlaying wet pad to facilitate the electrical contact. The wet pad also permitted E_{cor} measurements versus an externally applied SCE. The R_p values were obtained by imposing an anodic polarization of +10 mV versus E_{cor} for 300 s and by dividing this anodic overvoltage by the stable anodic current finally measured. Corrections for IR drop were not necessary because, as assessed by electrochemical impedance spectroscopy (EIS), the ohmic drop between the working and the inner reference electrodes was always negligible with respect to R_p values.

2.5.2. Electrochemical impedance spectroscopy tests

EIS spectra were collected at selected times, during the wet stage of the w/d cycles, by a Solartron apparatus (EI 1287, FRA 1260), combined with Zview software package. EIS measurements were performed at E_{cor} with ac perturbation ±10 mV and 5 measurements per decade. Spectra distortions at high frequencies (*hf*), likely connected to mortar non-homogeneities [29], restricted the frequency investigation in the range between 10^4 Hz (10^5 Hz for some spectra in geopolymers) and 10^{-3} Hz. The *hf* limitations prevented the analysis of the mortar dielectric properties.

2.5.3. Polarization curves

After 8, 43 and (in the case of REF) 100 days of exposure, in the wet stage of the w/d cycles, ohmic drop-compensated polarization curves were recorded, in order to better characterize the corrosion conditions

of the rebars. They were recorded at a scan rate of 0.166 mV s^{-1}, always starting from E_{cor}.

2.6. Corrosion product analysis

At the end of the exposure period, rebars not used for polarization curve recording were extracted from the mortars for visual observation and Raman analysis of surface corrosion products. Raman spectra were collected by a Renishaw Raman Invia instrument, under conditions that avoided the thermal degradation of iron compounds. An Ar + laser (514.5 nm) was adopted, with integration time (t) of 10 s, number of accumulations (n) of 4 and laser power (Pout) of 3 mW.

3. Results

3.1. Mortar characterization

Bulk density results, together with compressive strengths, elastic moduli and shrinkage values collected after 28 days of curing are reported in Table 1. These data evidence that REF mortar shows better mechanical performances and stability than geopolymers. In fact, it exhibits higher compressive strength values, higher E_d modulus and almost no shrinkage. Among geopolymers, G_1 has the best properties, in agreement with the information already available in the literature suggesting that the mechanical resistance of geopolymers increases at decreasing Na_2O/SiO_2 molar ratios [10,19]. G_1 shows a compressive strength value of 34.2 ± 2.9 MPa and can be classified as a 32.5 strength class binder, according to EN 196-1 [22]. With regard to shrinkage, a −0.3% variation was observed in G_1 and G_2, while a −0.1% was observed in G_3 mortar, which is the most stable geopolymeric formulation. The different curing conditions adopted for geopolymers (T = 25 °C and R.H. = 35%) and cement-based mortar (T = 25 °C and R.H. > 95%) partially explain the different shrinkage behaviour of geopolymers and REF. Shrinkage values for geopolymers higher than those usually exhibited by cement based mortars were already reported. This behaviour was also ascribed to loss of water from unreacted porous FA particles and to pore size distribution and relevant interconnectivity [30,31].

In order to justify the different physical–mechanical properties of REF and geopolymers, MIP was used to determine the pore distribution curves of the different mortars (Fig. 2). The total specific Hg volume intruded in geopolymer mortars, and particularly in G_3, was higher than that in REF, suggesting a higher total porosity and a greater vulnerability of geopolymers to degradation. More in detail, the pore size distribution curves of G_3 show the highest total porosity of about 85 mm^3/g (inducing the low measured bulk density of this mortar) and a bimodal pore size distribution positioned at about 1 μm and in the range 0.3–0.03 μm. The pore distribution curves of G_1 and G_2 are rather similar to each other and are characterized by a total porosity of 57–60 mm^3/g and pore radii mostly around 1–3 μm. In the case of REF, the total porosity is smaller (about 50 mm^3/g) and mainly consists in pores smaller than 0.5 μm and nanometric gel pores. As pores exceeding 1 μm are directly responsible for the rate of mass transfer through the porous system, the REF pore network will induce slower water saturation and mass transfer processes.

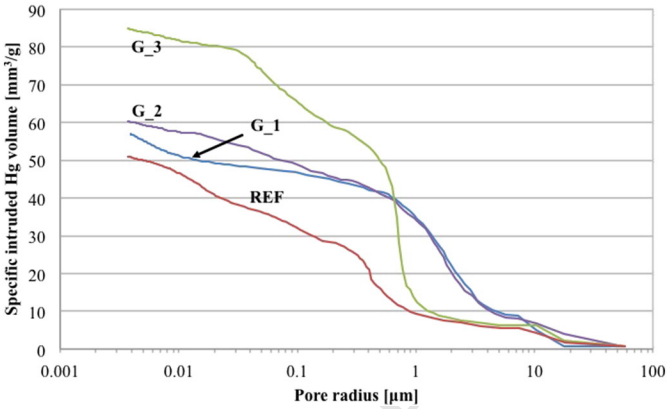

Fig. 2. Pore size distribution curves at 28 days of curing.

Apparent chloride diffusion coefficients, D_a, were also measured in the different mortars under fully saturated conditions to evaluate the relative chloride mobility under pure diffusion conditions, which is affected by pore dimensions, tortuosity and interconnectivity in the different porous systems. D_a of REF is smaller than those of geopolymers, which in turn increase going from G_1 to G_2 and G_3 (Table 2). The last value is one order of magnitude higher than that of REF. D_a data appear in good agreement with total porosity values.

3.2. pH and chloride content measurements

Table 3 collects the pH of the pore electrolytes measured in the core of unreinforced cylinders after 28 days of curing in the absence of carbonation (curing in plastic bags for geopolymers, normal curing for REF) and after 2 and 11 w/d cycles. The initial values obtained in the absence of carbonation in G_1 and G_2 are similar to those obtained in REF (12.80–12.97). Instead, G_3 exhibits a higher pH value (13.25), likely connected to the high Na_2O content in the activating solution.

During the w/d cycles, all FA mortar cylinders underwent a significant carbonation process. In particular, Table 3 evidences that the pH of the pore electrolyte in the cylinder cores decreased to about 12 after 14 days (2 cycles) and dropped to a common limit of 10.5–10.8, after 77 days (11 cycles). In contrast, the pH always remained well over 12 in the case of REF samples. This different behaviour is due to the formation of different reaction products after the reaction of the penetrated CO_2 with the alkaline components of the mortars: soluble sodium carbonate salts in geopolymers and insoluble calcium carbonate, capable to partially obstruct the mortar pores and to slow down the CO_2 penetration, in the case of REF [32]. The phenolphthalein test for carbonation depth assessment applied on the mortar cylinders after 14 days (2 cycles) (Fig. 3) confirmed that after this exposure time the cylinder cores were not carbonated. It also evidenced that no carbonation affected REF, while the carbonation depth decreased going from G_1 to G_2 and G_3 that is at increasing Na_2O/SiO_2 ratio in the activating solution. This suggests that a high Na_2O content can slightly slow down the carbonation rate.

The application of the standard ASTM method for the measurement of total chloride content in mortars after 2, 4, 6, 8, 11 w/d cycles

Table 1
Physical–mechanical characterization of the considered mortars after 28 days of curing.

Sample	Bulk density (g/cm^2)	Compressive strength (MPa)	Dynamic elastic modulus (GPa)	Shrinkage (%)
G_1	2.11 ± 0.01	34.2 ± 2.9	15.6 ± 1.7	−0.36 ± 0.13
G_2	2.07 ± 0.01	27.0 ± 3.1	15.9 ± 2.5	−0.37 ± 0.02
G_3	1.78 ± 0.13	22.5 ± 0.8	14.2 ± 2.2	−0.11 ± 0.02
REF	2.11 ± 0.02	47.0 ± 5.7	30.2 ± 2.2	−0.02 ± 0.01

Table 2
Apparent chloride diffusion coefficients in the different mortars.

Sample	D_a (m^2/s)
G_1	$9 \cdot 10^{-13}$
G_2	$1.6 \cdot 10^{-12}$
G_3	$3.6 \cdot 10^{-12}$
REF	$3 \cdot 10^{-13}$

Please cite this article as: C. Monticelli, et al., A study on the corrosion of reinforcing bars in alkali-activated fly ash mortars under wet and dry exposures to chloride solutions, Cem. Concr. Res. (2015), http://dx.doi.org/10.1016/j.cemconres.2016.05.010

Table 3
pH measurements for the investigated mortar samples.

Sample	pH after 28 d curing	pH after 2 w/d cycles	pH after 11 w/d cycles
G_1	12.80[a]	11.89	10.76
G_2	12.90[a]	11.96	10.54
G_3	13.25[a]	12.07	10.72
REF	12.97	12.66	12.18

[a] Curing in plastic bag, to assess initial pH in the absence of carbonation.

evidenced that chloride concentration was always independent of the depths in all mortar types. For this reason, Fig. 4 collects the average chloride contents measured inside the mortars, as a function of exposure time. In REF, the chloride content strongly augmented with time, reaching a concentration of 0.75 wt.% (vs binder) after 11 w/d cycles, while in FA samples, the average chloride content remained more or less constant during the exposure period, in the range of 0.06–0.18 wt.%, independently of the specific geopolymer considered. This different trend can be connected to differences in chloride binding capacity of the two mortar systems. In cement-based mortar, chlorides form low solubility calcium-containing compounds (e.g., Friedel salts, FS, calcium salts), while in geopolymers calcium content is low and the prevailing sodium chloride salt is characterized by a much higher leachability.

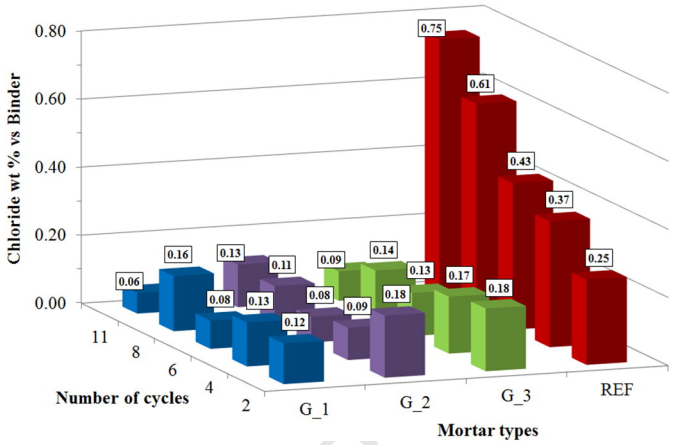

Fig. 4. Average total chloride contents (wt.% vs binder) in the investigated mortar samples after different exposure cycles.

3.3. Electrochemical tests

3.3.1. Potentiostatic R_p measurements

Fig. 5 collects representative time trends of E_{cor} and R_p values obtained in G_1 (a), G_2 (b), G_3 (c) and REF (d) mortars, during w/d cycles in 0.1 M NaCl solution. All of them clearly evidence the time at which rebar depassivation was achieved. In fact, initially, the rebar E_{cor} values were quite noble. They oscillated in the range −0.15/−0.06 V_{SCE} for G_3 and REF, while showed an increasing trend from about −0.17 to −0.10 V_{SCE}, in the case of G_1 and G_2. During this first period, R_p values of about 1 MΩ cm^2 or higher were recorded, with the highest values recorded in FA mortars. After 12–18 days, the E_{cor} values in geopolymers started to decrease and reached values of −0.60 V_{SCE} or more negative, while R_p values diminished progressively down to 1 kΩ cm^2, indicating the onset and propagation of a corrosion attack. In REF, the E_{cor} values of rebars started to decrease after longer exposure periods (longer than 40 days) and a concomitant sharp R_p drop was recorded, but afterwards the rebars again underwent repassivation/depassivation events, as denoted by the concurrent E_{cor}/R_p oscillations (Fig. 5d).

Corrosion in REF is connected to the penetration of chlorides (Fig. 4) that, after exposures of 42 days, arrive at concentrations of 0.43% (vs binder) and at the end of the exposure period reach concentrations of 0.75% (vs binder). These chloride levels are comparable or higher than those reputed critical for the onset of corrosion in traditional non-carbonated mortars [33]. In geopolymers, in spite of the smaller amounts of penetrated chlorides, rebar depassivation was detected at shorter times. This is reasonably connected to the quick mortar carbonation, which decreased the mortar pH and for this reason reduced the critical chloride contents for the onset of corrosion. However, in geopolymers a low calcium content is present which is expected to reduce the formation of insoluble chloride salts, so increasing the fractions of free to total chloride concentrations. Therefore, in spite of the low detected total chloride contents, relatively high amounts of aggressive free chlorides cannot be excluded.

Fig. 6 shows the relationship between R_p and E_{cor} for the different mortars, independently of exposure time. As expected from Fig. 5, higher R_p mainly corresponded to nobler E_{cor} values in all mortars and time evolution, indicated in the Figure, confirmed progression towards rebar corrosion, in the timeframe of the tests here described. However, in geopolymers passive conditions (that is conditions with noble E_{cor} values) corresponded to higher R_p, in comparison to REF. This was likely connected to the relevant amounts of silicates present in the pore electrolyte of geopolymers, which could slightly inhibit the corrosion process and reinforce passivity, as found in a previous research [10]. As a result, the linear trends fitting log R_p/E_{cor} values in G_1 and G_2 (Fig. 6) had higher slopes than that of REF. In the case of G_3, the rebar behaviour was the same detected in G_1 and G_2 at the beginning of the test (that is under passive conditions), but during depassivation R_p values higher than those measured in the other geopolymers were detected. When severe corrosion conditions were reached (green diamonds with the more negative E_{cor} values in Fig. 6), the R_p of the rebars in G_3 became similar to those found in the other geopolymers. The relatively high R_p values detected in this geopolymer for some time during depassivation are likely connected to its high Na_2O content, which can

Fig. 3. Carbonation depth assessment (by phenolphthalein method) on sectioned mortar cylinders exposed for 14 days (2 cycles) to the 0.1 M NaCl solution.

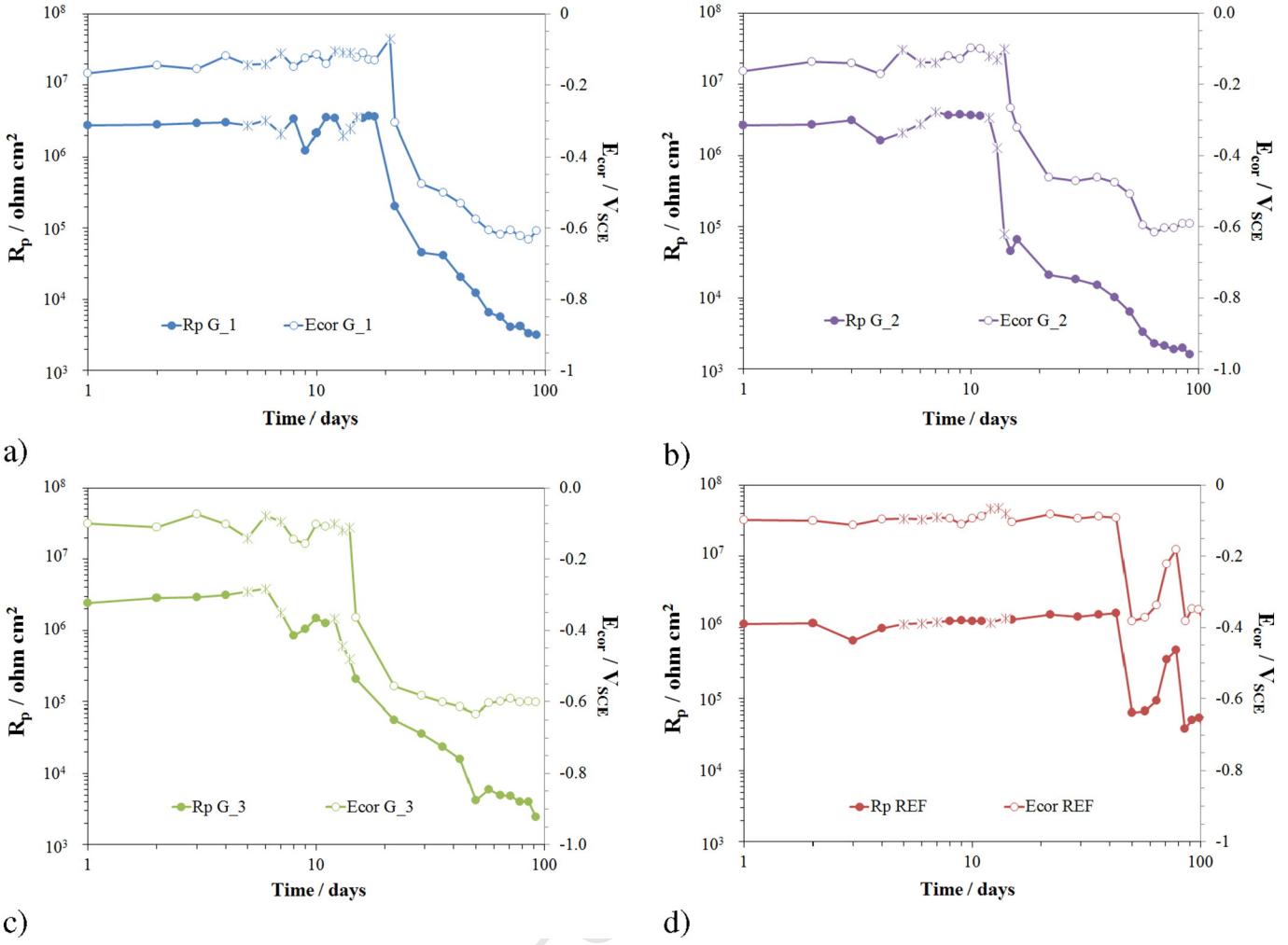

Fig. 5. Representative time trends of the corrosion potential and polarization resistance values obtained in G_1 (a), G_2 (b), G_3 (c) and REF (d) mortars, during w/d cycles in 0.1 M NaCl solution. Most data were obtained during the wet step of the cycles. Those collected in the dry step are indicated by the symbol *.

slow down carbonation and pH diminution and, for a while, can favour slightly lower corrosion rates.

Fig. 6 describes the R_p/E_{cor} dependence during depassivation, but it does not give any information about the speed of depassivation. In order to compare the depassivation rate in the different mortar types on a statistical basis, Fig. 7 shows the time evolution of the fraction of rebars with corrosion probability greater than 90%, that is the fraction of rebars characterized by E_{cor} values more negative than −0.276 V_{SCE} [27]. The figure clearly evidences that REF offers the highest corrosion protection to the reinforcements, as an exposure period longer than

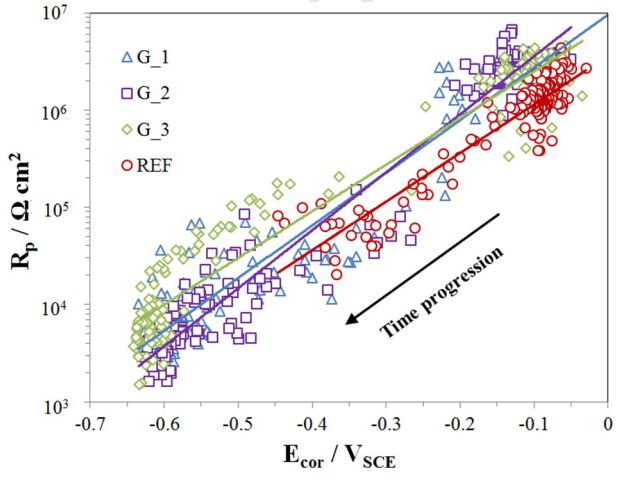

Fig. 6. Relations between R_p and E_{cor} measured during w/d exposures in the different mortars.

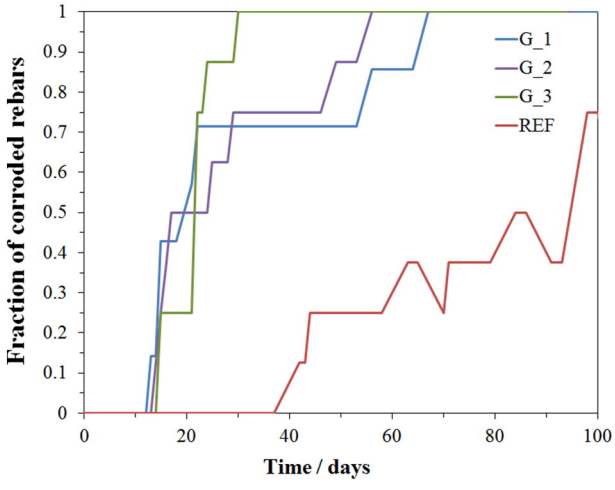

Fig. 7. Time dependence of the rebar fractions affected by corrosion in the different mortars during w/d cycles in 0.1 M NaCl solution.

Please cite this article as: C. Monticelli, et al., A study on the corrosion of reinforcing bars in alkali-activated fly ash mortars under wet and dry exposures to chloride solutions, Cem. Concr. Res. (2015), http://dx.doi.org/10.1016/j.cemconres.2016.05.010

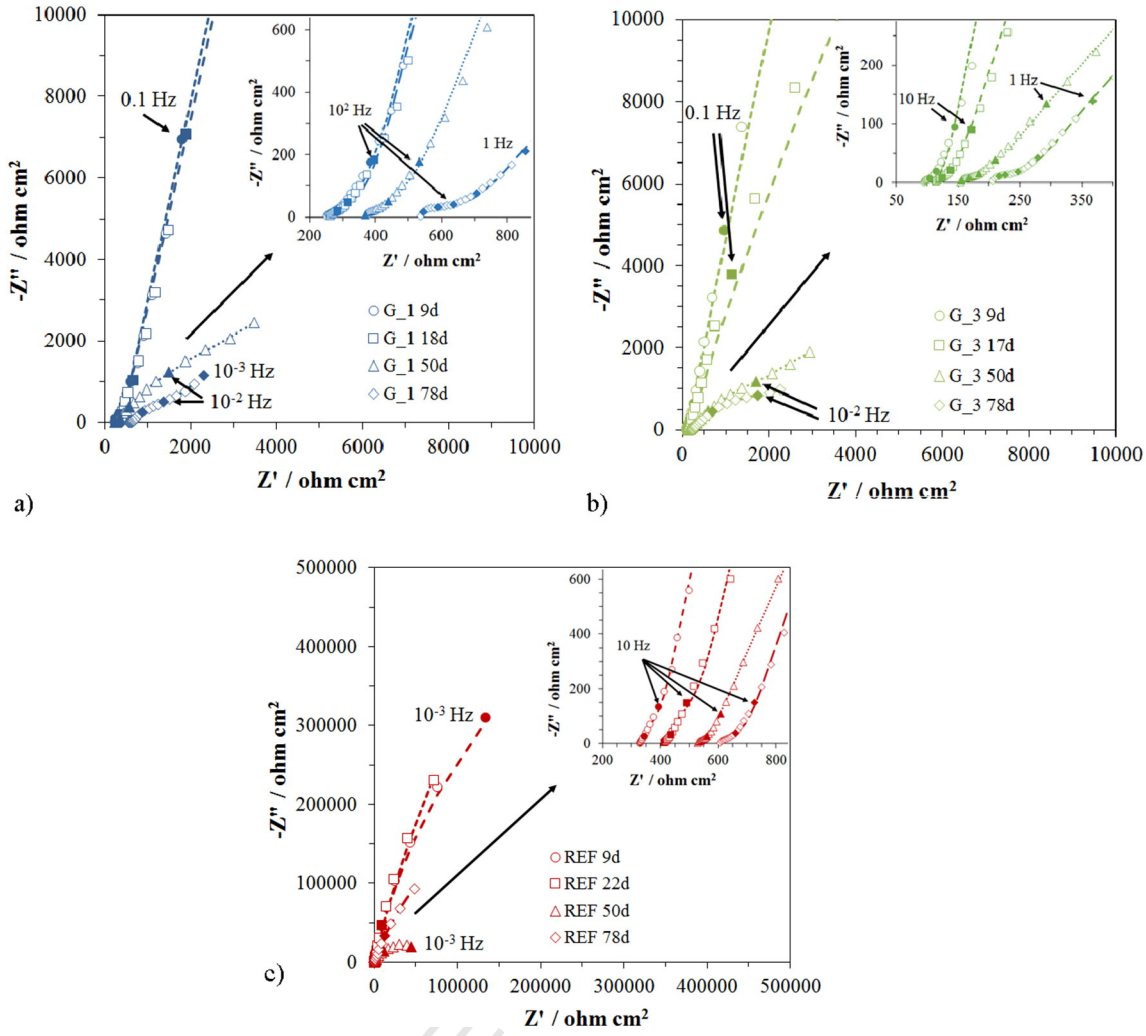

Fig. 8. Experimental (symbols) and simulated (lines) EIS spectra recorded in G_1 (a), G_3 (b) and REF (c) mortars at different exposure times. Solid symbols refer to the first frequency of each decade.

95 days is necessary to induce corrosion attack on more than 50% of the rebars. In the case of geopolymers this occurs after about 20 days. In G_1 and G_2, corrosion propagates in all rebars after about 60 days, while in G_3 this occurs after only 25 days. This suggests that the high G_3 porosity (Fig. 2) permits a faster oxygen diffusion (and faster corrosion) and contrasts the positive effects of a slower carbonation rate.

3.3.2. Electrochemical impedance spectroscopy

The EIS spectra collected in G_1 and G_3 geopolymers at different exposure times are shown in Fig. 8a and b in the form of Nyquist plots. Those obtained in G_2 are quite similar and have not been shown.

Before the onset of corrosion, identified by R_p and E_{cor} drops (Fig. 5), the spectra comprised two capacitive loops. The first one, at frequencies higher than 10^2 Hz, was very small and often ill-resolved, particularly at short immersion times (boxes in Fig. 8a,b). Different interpretations were given to it (film of corrosion products [34], presence of a cementitious film on the rebar surface, with specific characteristics different from that of bulk mortars [35,36]). As its presence was observed since the beginning of the exposures, when the rebars were still passive, the last interpretation connecting it to dielectric properties of an interfacial geopolymeric region appears correct. The second capacitive arc at frequencies lower than 10^2–10 Hz was connected to charge transfer reactions on the rebar surface.

These spectra were reasonably well fitted by the equivalent circuit (EC) in Fig. 9a [9,37–39] and the obtained simulated curves are superimposed on the experimental spectra of Fig. 8. The first element in the EC is the resistance R_{s+m}, which corresponds to the sum of the pore electrolyte and mortar resistance between the pseudo-reference Ti electrode and the steel surface. Then, the EC shows two parallel combinations of a resistance (R) and a constant phase element (CPE), in

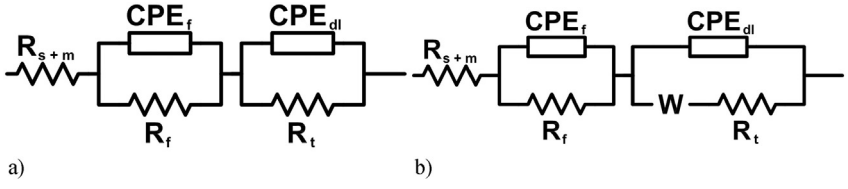

Fig. 9. Equivalent circuits used to fit EIS spectra: a) under passive conditions or limited corrosion attack; b) under active corrosion conditions.

Please cite this article as: C. Monticelli, et al., A study on the corrosion of reinforcing bars in alkali-activated fly ash mortars under wet and dry exposures to chloride solutions, Cem. Concr. Res. (2015), http://dx.doi.org/10.1016/j.cemconres.2016.05.010

series to each other. The first combination (R_f-CPE_f arm) fits the *hf* shoulder connected to the presence of the interface mortar film [38], while the low frequency (*lf*) combination (R_t-CPE_{dl}) is linked to the charge transfer resistance and double layer capacitance and gives information on the corrosion process. In EC, the substitution of capacitances with Constant Phase Elements (CPE) aims at complying with inhomogeneities and discontinuities at interfaces. CPE is a distributed element with impedance expression:

$$Z_{CPE} = \left[Y(j\omega)^n\right]^{-1} \quad (1)$$

where $Y(j\omega)^n$ is an admittance, j is the imaginary unit, ω is the angular frequency, $0 \le n \le 1$ (for $n = 0$ CPE stands for a resistance, while for $n = 1$ it is a pure capacitance).

In the presence of a severe corrosion attack (very negative E_{cor} and low potentiostatic R_p values), impedance spectra were characterized by three capacitive arcs (Fig. 8a,b). Beside the *hf* one, related to the interfacial mortar film, two other arcs were present, connected to charge transfer (the medium frequency, *mf*, arc) and mass transfer (*lf* arc) processes. These spectra were correctly fitted by the EC of Fig. 9b [9,37,39,40], where in the R_t-CPE_{dl} arm a Finite-Length Warburg element (W) was introduced to take into account the influence of diffusion on corrosion:

$$W = R_w \cdot \frac{\tanh\left[j\omega\left(\frac{\delta^2}{D}\right)\right]^P}{\left[j\omega\left(\frac{\delta^2}{D}\right)\right]^P} \quad (2)$$

where δ is the effective diffusion path length, D the effective diffusion coefficient and $0 \le P \le 1$ [39,41].

The fitting parameters related to all geopolymer spectra are reported in Tables 4–6. R_{s+m} values are always very small, in the range 70–500 Ω cm^2, given the position of the reference electrode in close proximity of the steel electrode, and tend to increase with time, likely due to the going on of the mortar curing. As the chloride content in the mortars is more or less constant with time, also the observed increase with time of the geopolymeric interfacial film resistance (R_f) could be connected to the time evolution of the mortar compactness. The pore obstruction with corrosion products in the proximity of the rebars could give a further contribution to R_f increase at times longer than 20 days. Differences in R_{s+m} and R_f among geopolymers confirm the higher compactness of G_1 in comparison to the other FA mortar formulations. At short exposure periods, R_t values are higher (and often much higher) than 1 MΩ cm^2, meaning that charge transfer through the surface passive films controls the corrosion rates. When E_{cor} values become more negative and set within −0.3/−0.6 V_{SCE}, R_t values decrease concurrently, down to some kΩ cm^2 and double layer pseudo capacitances significantly increase up to a few mΩ^{-1} cm^{-2} s^{ndl}. These variations are connected, respectively, to the decrease of surface oxide film protectiveness and to the increase in real surface area of corroded rebars. Under severe corrosion conditions, the Warburg parameter R_W, representing the resistance to diffusion processes, has always the same magnitude order of R_t, suggesting that corrosion rate is under a mixed charge transfer/diffusion control. G_3 presents slightly lower R_W and (δ^2/D) values, likely due to the lower resistance to diffusion and higher diffusion coefficient in the most porous G_3 microstructure.

The EIS spectra obtained in REF mortar are collected in Fig. 8c. They are quite similar to those collected in geopolymers before the development of severe corrosion, suggesting that in this case diffusion phenomena do not affect the corrosion rates. Therefore, only the EC of Fig. 9a was adopted to fit the experimental spectra and the results are collected in Table 7. The R_{s+m} are slightly higher than those measured in the most compact geopolymer (G_1), in agreement with the even denser REF microstructure. Also in REF, a continuous increase with time of R_{s+m} and R_f values is recorded, in spite of chloride accumulation, due to the prevailing effect of the ongoing mortar curing. The more long lasting protectiveness of REF reflects in the persistence of relatively high R_t values till the end of the test and in the capability of steel repassivation, after the onset of a corrosion attack. In fact, after 50 days R_t decreases to 60 kΩ cm^2 (and E_{cor} diminishes to −0.38 V_{SCE}) and then, after 78 days, it increases again up to 600 kΩ cm^2 (and E_{cor} ennobles up to −0.18 V_{SCE}).

3.3.3. Polarization curves

Fig. 10 shows the ohmic drop-compensated polarization curves recorded on reinforcing bars in geopolymers (Fig. 10a) and REF (Fig. 10b). They clearly evidence that at increasing exposure periods, variations in surface film stability (connected to the pore solutions modifications described in Section 3.2) modify the rebar electrochemical behaviour. In particular, the curves show that after 8 days exposure stable passive films are present in both mortar types, inducing noble E_{cor} (around −0.1 V_{SCE}) and low i_{cor} values (varying within 0.06–0.1 μA/cm^2). Passive currents are recorded up to potentials of about +0.6 V_{SCE} where an abrupt current increase was observed, due to oxygen evolution [42]. Instead, after 43 days, the polarization curves recorded in geopolymers (Fig. 10a) exhibited much more negative E_{cor}

Table 5
Fitting parameters of EIS spectra and related E_{cor} values, obtained in G_2 mortar.

Time/days	2	9	16	50	78
E_{cor}/V_{SCE}	−0.137	−0.128	−0.322	−0.596	−0.606
R_{s+m}/Ω cm^2	124	140	143	227	423
R_f/Ω cm^2	40	70	53	40	100
$Y_f/\mu\Omega^{-1}$ cm^{-2} s^{nf}	800	800	800	700	226
n_f	0.53	0.5	0.5	0.5	0.5
R_t/kΩ cm^2	5300	10,000	40.5	3.8	1.36
R_W/kΩ cm^2		–	–	4.42	2.00
δ^2/D/s		–	–	968	673
P		–	–	0.5	0.5
$Y_{dl}/\mu\Omega^{-1}$ cm^{-2} s^{ndl}	230	221	316	1800	2240
n_{dl}	0.88	0.87	0.8	0.6	0.57

Table 4
Fitting parameters of EIS spectra and related E_{cor} values, obtained in G_1 mortar.

Time/days	2	9	18	50	78
E_{cor}/V_{SCE}	−0.128	−0.141	−0.13	−0.575	−0.621
R_{s+m}/Ω cm^2	165	250	250	360	520
R_f/Ω cm^2	64	150	150	220	220
$Y_f/\mu\Omega^{-1}$ cm^{-2} s^{nf}	300	370	320	540	360
n_f	0.6	0.53	0.5	0.42	0.40
R_t/kΩ cm^2	6000	16,000	20,000	5.26	1.86
R_W/kΩ cm^2		–	–	5.97	2.64
δ^2/D/s		–	–	500	650
P		–	–	0.5	0.5
$Y_{dl}/\mu\Omega^{-1}$ cm^{-2} s^{ndl}	200	200	196	3740	3919
n_{dl}	0.87	0.87	0.87	0.65	0.6

Table 6
Fitting parameters of EIS spectra and related E_{cor} values, obtained in G_3 mortar.

Time/days	2	9	17	50	78
E_{cor}/V_{SCE}	−0.134	−0.156	−0.364	−0.634	−0.601
R_{s+m}/Ω cm^2	71	96	114	154	205
R_f/Ω cm^2	15	34	35	51	69
$Y_f/\mu\Omega^{-1}$ cm^{-2} s^{nf}	600	600	821	878	463
n_f	0.6	0.5	0.5	0.5	0.5
R_t/kΩ cm^2	4500	1150	220	3.50	2.50
R_W/kΩ cm^2	–	–	–	4.5	1.51
δ^2/D/s	–	–	–	270	193
P	–	–	–	0.5	0.5
$Y_{dl}/\mu\Omega^{-1}$ cm^{-2} s^{ndl}	266	297	370	1960	1800
n_{dl}	0.89	0.885	0.82	0.63	0.65

Please cite this article as: C. Monticelli, et al., A study on the corrosion of reinforcing bars in alkali-activated fly ash mortars under wet and dry exposures to chloride solutions, Cem. Concr. Res. (2015), http://dx.doi.org/10.1016/j.cemconres.2016.05.010

Table 7
Fitting parameters of EIS spectra and related E_{cor} values, obtained in REF mortar.

Time/days	2	9	22	50	78
E_{cor}/V_{SCE}	−0.098	−0.11	−0.082	−0.382	−0.181
$R_{s+m}/\Omega\ cm^2$	238	328	416	525	600
$R_f/\Omega\ cm^2$	57	57	60	80	100
$Y_f/\mu\Omega^{-1}\ cm^{-2}\ s^{nf}$	200	200	200	200	200
n_f	0.9	0.9	0.85	0.64	0.56
$R_t/k\Omega\ cm^2$	1200	1500	2500	60	600
$Y_{dl}/\mu\Omega^{-1}\ cm^{-2}\ s^{ndl}$	258	243	235	381	262
n_{dl}	0.89	0.88	0.87	0.76	0.81

(in the range −0.5/−0.6 V_{SCE}) and much higher i_{cor} values (about 3–4 μA/cm^2). Under these conditions, high pseudo-passive currents (higher than 10^{-5} A/cm^2) were recorded, slowly increasing from E_{cor} up to the potential of oxygen evolution, without discontinuity. This curve suggests a degradation of surface film protectiveness which permits significant corrosion at E_{cor}.

The conditions detected in REF after the same exposure time (43 days) are quite different. In fact, the curves show E_{cor} and i_{cor} values close to those measured after 8 days (Fig. 10b), suggesting the permanence of passive conditions at E_{cor}. However, an abrupt current increase was recorded at about +0.135 V_{SCE}, due to pitting attack [11]. This means that the surface film has a smaller resistance towards anodic polarization, owing to chloride accumulation (Fig. 4). After 100 days of exposure, a stronger corrosion attack affected the rebars already at E_{cor} (i_{cor} of about 2 μA/cm^2) and rebars were under pseudo-passive conditions. Anyway, i_{cor} remained smaller than those obtained in geopolymers after 43 days.

3.4. Corrosion product analysis

At the end of the w/d cycles, rebars not used for polarization curve recording were extracted from the mortars to visualize the extent of the corrosion attack and investigate the nature of the corrosion products. In agreement with the suggestions of electrochemical tests, a more widespread corrosion attack was found in FA mortars in comparison to REF, as shown in Fig. 11.

Table 8 reports the results of Raman analysis of corrosion products formed on the steel surface at the end of the w/d cycles. A range of diverse amorphous and crystalline oxide structures was found, but abundance of Akaganeite (β-FeO(OH,Cl)) was detected only in geopolymers with the characteristic *cotton balls* and *rosette* shapes [43]. In REF, the most abundant crystalline compound was lepidocrocite (γ-FeO(OH)), while maghemite (γ-Fe_2O_3) and goethite (α-FeO(OH) were found in traces. Those results are in agreement with the severe corrosion attack detected in geopolymers by the electrochemical tests. In particular, the presence of agakaneite confirms the chloride incorporation in the oxide structure, with the formation of a very scarcely protective surface film [44]. Similar results were also found in [10].

4. Discussion of the results

In this research, the adoption of decreasing Na_2O/SiO_2 ratios in the activating solution produced geopolymers with more compact microstructures and higher compressive strength values and elastic moduli (Table 1). G_1 showed the best mechanical properties and, consistently, the highest stability and the lowest apparent diffusion coefficient for chlorides among geopolymers (Tables 1 and 2), even if it remained less performant than REF.

In particular, a higher scale porosity was detected in geopolymers, which can be ascribed to the different nature of the gels formed during hardening in these mortar types, in comparison to REF. In fact, whereas C–S–H is the main product usually formed in the latter mortar type, binding phases formed by alkali activation of FA are generally constituted by gels such as C–A–S–H, N–A–S–H and C–S–H, depending on the precursor chemical composition [20,45,46]. The pores associated with C–A–S–H and N–A–S–H gel are larger, mainly due to FA grain dissolution after alkali activation, even if they are often accessed via narrow constrictions caused by ink-bottle pores [47,48]. It is well known that the mortar porosity is the pathway through which aggressive species, such as oxygen, chlorides and carbon dioxide, penetrate and induce variations in pore electrolyte composition and corrosion attack on the reinforcing bars.

In REF, after 77 days chloride concentrations of 0.75% vs binder were measured, that are in the range of those reputed critical for corrosion onset in non-carbonated mortars (Fig. 4, [33]). These high chloride concentrations are mainly bound to the mortar gels as low solubility calcium-containing compounds (e.g., Friedel salts, calcium chloride), which represent a reservoir of aggressive chloride ions. Consequently, after 95 days 50% of the rebars in REF suffered active corrosion (Fig. 7).

In FA mortars, corrosion affected 50% of the rebars after only 20 days (Fig. 7), in spite of their much lower measured chloride content (Fig. 4). The limited total chloride concentrations are due to the formation of highly soluble alkali metal salts, so that external chlorides can easily penetrate but can also be easily leached out during w/d cycles. However, under these conditions, a relatively high fraction of free aggressive chlorides is likely present and available to stimulate the rebar corrosion attack. In addition, a fast carbonation was found to affect geopolymers, which is also capable to impair rebar passivity (Fig. 3 and Table 3). The consequent pH drop in the pore electrolyte causes a decrease in the critical chloride concentration, so that lower chloride concentrations are needed to start corrosion. Geopolymer carbonation was found to

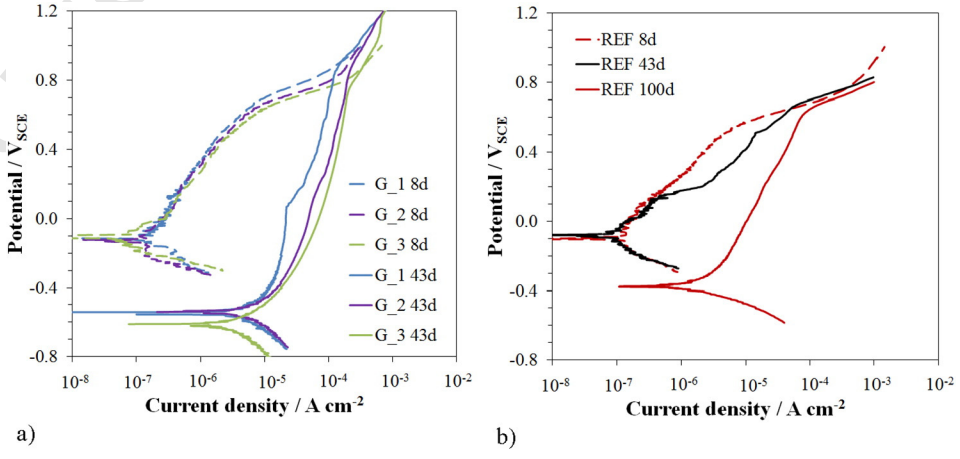

Fig. 10. Polarization curves recorded in the different mortars during the wet step of w/d cycles in 0.1 M NaCl solution.

Please cite this article as: C. Monticelli, et al., A study on the corrosion of reinforcing bars in alkali-activated fly ash mortars under wet and dry exposures to chloride solutions, Cem. Concr. Res. (2015), http://dx.doi.org/10.1016/j.cemconres.2016.05.010

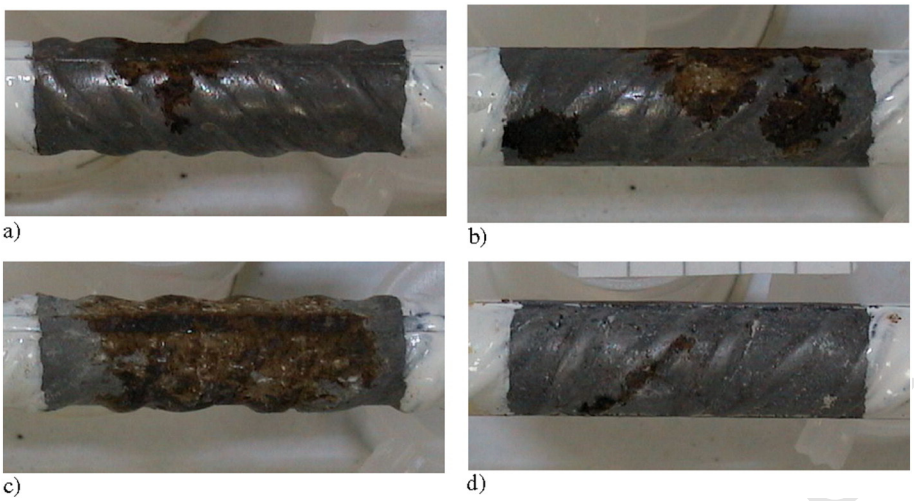

Fig. 11. Extent of corrosion attack on steel bars extracted from samples at the end of electrochemical tests: a) G_1; b) G_2; c) G_3; d) REF.

depend on the Na_2O/SiO_2 ratio in the activating solution, so that G_1 was the most affected geopolymer, while G_3 was the most resistant to pH variation (Fig. 3). However, the quite porous G_3 microstructure had an overwhelming influence in corrosion stimulation.

The EIS spectra analysis gave results in good agreement with these observations. They clearly evidence that at each exposure time, the mortar compactness (and R_{s+m} values) was highest in REF. The *hf* loop, describing the dielectric properties of the interfacial mortar region in contact with the rebars, showed R_f values depending on both the mortar porosity and the abundance of corrosion products inside the mortar pores. Therefore, the densest REF mortar reached intermediate R_f values, because of a limited accumulation of corrosion products in the mortar region close to the rebar surface.

At frequencies lower than 10^2–10 Hz, the spectra described the corrosion processes affecting the embedded rebars. In REF, the spectra always showed the persistence of a single *lf* arc, with relatively high R_t values, indicative of the persistence of passivity or pseudopassivity on the rebars. In geopolymers, severe corrosion attack developed with time, as indicated by the appearance of a second *lf* capacitive arc, suggesting a mixed charge transfer/diffusion control on the corrosion rate.

5. Conclusions

During this research, the corrosion behaviour of rebars embedded in RT-cured geopolymer mortars based on class F FA was assessed during w/d exposure to 0.1 M NaCl solution and it was compared to that shown by rebars in a traditional cement-based mortar under the same aggressive conditions. The differences detected were interpreted in the light of chemical, physical and microstructural differences found in the two systems.

In particular, the results achieved suggested that:

- in geopolymers, a low Na_2O/SiO_2 ratio in the activating solution permitted to achieve the densest microstructure and the best physical–mechanical properties. However, geopolymer performances were inferior to those of REF;
- under w/d exposure conditions, all geopolymers suffered a quick mortar carbonation, which was reputed responsible of a fast rebar depassivation, in spite of a low total chloride concentration accumulated around the rebars. Instead, REF was more protective as it did not suffer any carbonation.
- fitting of EIS spectra recorded at intervals gave information in good agreement with E_{cor}/R_p measurements and permitted to monitor the evolution of the dielectric properties of interfacial mortar films and electrochemical and mass transport processes affecting passive and corroding rebars.

Acknowledgements

The authors wish to thank Dr. F. Lolli for her useful assistance in microstructural and mechanical characterizations, Dr. M. Abbottoni for his valuable assistance in performing part of the electrochemical measurements and Dr. R. Gaiba for his precious analytical support.

References

[1] M.S. Imbabi, C. Carrigan, S. McKenna, Trends and developments in green cement and concrete technology, Int. J. Sust. Built Env. 1 (2012) 194–216.
[2] J.L. Provis, Geopolymers and other alkali-activated material: why, how and what? Mater. Struct. 47 (2014) 11–25.
[3] P. Duxson, J.L. Provis, G.C. Lukey, S.W. Mallicoat, W.M. Kriven, J.S.J. van Deventer, Understanding the relationship between geopolymer composition, microstructure and mechanical properties, Colloids Surf. A Physicochem. Eng. Asp. 269 (2005) 47–58.
[4] J.L. Provis, A. Palomo, C. Shi, Advances in understanding alkali-activated materials, Cem. Concr. Res. 78 (2015) 110–125.
[5] F. Pacheco-Torgal, Z. Abdollahnejad, A.F. Caomoes, M. Jamshidi, Y. Ding, Durability of alkali-activated binders: a clear advantage over Portland cement or an unproven issue? Constr. Build. Mater. 30 (2012) 400–405.
[6] B. Singh, G. Ishwarya, M. Gupta, S.K. Bhattacharyya, Geopolymer concrete: a review of some recent developments, Constr. Build. Mater. 85 (2015) 78–90.

Table 8
Raman quantitative analysis for corrosion products formed on rebars in reinforced cylinders at the end of the w/d cycles (+/− = traces; + = small amounts detected; ++ = high amounts detected).

Sample	Lepidocrocite	Maghemite	Akaganeite	Goethite	δ-FeOOH
G_1	+/−		++		+/−
G_2		+/− (amorphous)	+ (amorphous)	+/− (amorphous)	
G_3		+ (amorphous)	++		
REF	+	+/−		+/−	

[7] M.M. Hossain, M.R. Karim, M.K. Hossain, M.N. Islam, M.F.M. Zain, Durability of mortar and concrete containing alkali-activated binder with pozzolans: a review, Constr. Build. Mater. 93 (2015) 95–109.

[8] A. Neville, Chloride attack of reinforced concrete: an overview, Mater. Struct. 28 (1995) 63–70.

[9] M. Criado, S. Martínez-Ramirez, S. Fajardo, P.P. Gómez, J.M. Bastidas, Corrosion rate and corrosion product characterisation using Raman spectroscopy for steel embedded in chloride polluted fly ash mortar, Mater. Corros. 64 (5) (2013) 372–380.

[10] C. Monticelli, M.E. Natali, A. Balbo, C. Chiavari, F. Zanotto, S. Manzi, M.C. Bignozzi, Corrosion behavior of steel in alkali-activated fly ash mortars in the light of their microstructural, mechanical and chemical characterization, Cem. Concr. Res. 80 (2016) 60–68.

[11] C. Monticelli, M. Criado, S. Fajardo, J.M. Bastidas, M. Abbottoni, A. Balbo, Corrosion behavior of a low Ni austenitic stainless steel in carbonated chloride-polluted alkali-activated fly ash mortars, Cem. Concr. Res. 55 (2014) 49–58.

[12] F.U.A. Shaikh, Effects of alkali solutions on corrosion durability of geopolymer concrete, Adv. Concr. Constr. 2 (2) (2014) 109–123.

[13] D.M. Bastidas, A. Fernández-Jiménez, A. Palomo, J.A. González, A study on the passive state stability of steel embedded in activated fly ash mortars, Corros. Sci. 50 (2008) 1058–1065.

[14] J.L. Thompson, B.E. Scheetz, M.R. Schock, D.A. Lytle, P.J. Delaney, Sodium silicate corrosion inhibitors: issues of effectiveness and mechanisms, Proc. Water Quality Technology Conference, November 9–12, 1997, Denver, CO.

[15] J.T. Gourley, G.B. Johnson, Developments in geopolymer precast concrete in geopolymer, green chemistry and sustainable development solutions, in: J. Davidovits (Ed.), Proc. World Congress Geopolymer 2005 2005, pp. 139–143.

[16] J.M. Miranda, A. Fernández-Jiménez, J.A. González, A. Palomo, Corrosion resistance in activated fly ash mortars, Cem. Concr. Res. 35 (2005) 1210–1217.

[17] J.S.J. van Deventer, J.L. Provis, P. Duxson, Technical and commercial progress in the adoption of geopolymer cement, Miner. Eng. 29 (2012) 89–104.

[18] J. Temuujin, R.P. Williams, A. van Riessen, Effect of mechanical activation of fly ash on the properties of geopolymer cured at ambient temperature, J. Mater. Process. Technol. 209 (2009) 5276–5280.

[19] N.K. Lee, H.K. Lee, Setting and mechanical properties of alkaliactivated fly ash/slag concrete manufactured at room temperature, Constr. Build. Mater. 47 (2013) 1201–1209.

[20] M.C. Bignozzi, S. Manzi, M.E. Natali, W.D.A. Richard, A. van Riessen, Room temperature alkali activation of fly-ash: the effect of Na_2O/SiO_2 ratio, Constr. Build. Mater. 69 (2014) 262–270.

[21] P. Nath, P.K. Saker, Use OPC to improve setting and early stregth properties of low calcium fly ash geopolymer concrete cured at room temperature, Cem. Concr. Compos. 55 (2015) 205–214.

[22] EN 196-1, Methods of Testing Cement — Part 1: Determination of Strength, 2005.

[23] EN 12617-4, Products and Systems for the Protection and Repair of Concrete Structures – Test Methods – Determination of Shrinkage and Expansion, 2003.

[24] DIN 66133, Determination of Pore Volume Distribution and Specific Surface Area of Solids by Mercury Intrusion, 1993.

[25] ASTM, C1556. Standard Test Method for Determinig the Apparent Chloride Diffusion Coefficient of Cementitious Mixtures by Bulk Diffusion, 2003.

[26] ASTM C1152/C1152M, Standard Test Method for Acid-soluble Chloride in Mortar and Concrete, 2004.

[27] ASTM C114, Standard Test Methods for Chemical Analysis of Hydraulic Cement, 2011.

[28] V. Räsänen, V. Penttala, The pH measurement of concrete and smoothing mortar using a concrete powder suspension, Cem. Concr. Res. 34 (2004) 813–820.

[29] M. Serdar, L. Valek Žulj, D. Bjegović, Long-term corrosion behaviour of stainless reinforcing steel in mortar exposed to chloride environment, Corros. Sci. 69 (2013) 149–157.

[30] T. Xie, T. Ozbakkaloglu, Behavior of low-calcium fly and bottom ash-based geopolymer concrete cured at ambient temperature, Ceram. Int. 41 (2015) 5945–5958.

[31] F. Collins, J.G. Sanjayan, Effect of pore size distribution on drying shrinkage of alkali activated slag concrete, Cem. Concr. Res. 30 (2000) 1401–1406.

[32] M. Fernandez Bertos, S.J.R. Simons, C.D. Hills, P.J. Carey, A review of accelerated carbonation technology in the treatment of cement-based materials and sequestration of CO_2, J. Hazard. Mater. B112 (2004) 193–205.

[33] U. Angst, B. Elsener, C.K. Larsen, G.C. Luckey, Ø. Vennesland, Critical chloride content in reinforced concrete — a review, Cem. Concr. Res. 39 (2009) 1122–1138.

[34] M. Ismail, M. Ohtsu, Corrosion rate of ordinary and high-performance concrete subjected to chloride attack by AC impedance spectroscopy, Constr. Build. Mater. 20 (2006) 458–469.

[35] M.F. Montemor, M.P. Simoes, M.M. Salta, M.G.S. Ferreira, The assessment of the electrochemical behaviour of fly ash-containing concrete by impedance spectroscopy, Corros. Sci. 35 (1993) 1571–1578.

[36] M. Keddam, H. Takenouti, X.R. Nóvoa, C. Andrade, C. Alonso, Impedance measurements on cement paste, Cem. Concr. Res. 27 (1997) 1191–1201.

[37] V. Feliu, J.A. Gonzalez, C. Andrade, S. Feliu, Equivalent circuit for modelling the steel-concrete interface. I. Experimental evidence and theoretical predictions, Corros. Sci. 40 (1998) 975–993.

[38] P. Gu, S. Elliot, J.J. Beaudoin, B. Arsenault, Corrosion resistance of stainless steel in chloride contaminated concrete, Cem. Concr. Res. 26 (1996) 1151–1156.

[39] L. Yohai, M.B. Valcarce, M. Vázquez, Testing phosphate ions as corrosion inhibitors for construction steel in mortars, Electrochim. Acta 202 (2016) 316–324.

[40] K.K. Sagoe-Crentsil, F.P. Glasser, J.T.S. Irvine, Electrochemical characteristics of reinforced concrete corrosion as determined by impedance spectroscopy, Br. Corros. J. 27 (1992) 113–118.

[41] G. Trabanelli, C. Monticelli, V. Grassi, A. Frignani, Electrochemical study on inhibitors of rebar corrosion in carbonated concrete, Cem. Concr. Res. 35 (2005) 1804–1813.

[42] E. Volpi, A. Olietti, M. Stefanoni, S.P. Trasatti, Electrochemical characterization of mild steel in alkaline solutions simulating concrete environment, J. Electroanal. Chem. 736 (2015) 38–46.

[43] J.D. Moreno, M. Bonilla, J.M. Adam, M.V. Borrachero, L. Soriano, Determining corrosion levels in the reinforcement rebars of buildings in costal areas. A case study in the Mediterranean coastline, Constr. Build. Mater. 100 (2015) 11–21.

[44] P. Refait, J.M.R. Genin, The mechanisms of oxidation of ferrous hydroxychloride β-$Fe_2(OH)_3Cl$ in aqueous solution: the formation of akaganeite vs goethite, Corros. Sci. 33 (1993) 539–553.

[45] I. Ismail, S.A. Bernal, J.L. Provis, R. San Nicolas, D.G. Brice, A.R. Kilcullen, et al., Influence of fly ash on the water and chloride permeability of alkali activated slag mortars and concrete, Constr. Build. Mater. 48 (2013) 1187–1201.

[46] I. Garcia-Lodeiro, A. Palomo, A. Fernández-Jiménez, D.E. Macphee, Compatibility studies between N–A–S–H and C–A–S–H gels. Study in the ternary diagram Na_2O–CaO–Al_2O_3–SiO_2–H_2O, Cem. Concr. Res. 41 (2011) 923–931.

[47] Y. Ma, J. Hu, G. Ye, The pore structure and permeability of alkali activated fly ash, Fuel 104 (2013) 771–780.

[48] R.R. Lloyd, J.L. Provis, K.J. Smeaton, J.S.J. van Deventer, Spatial distribution of pores in fly ash-based inorganic polymer gels visualized by Wood's metal intrusion, Microporous Mesoporous Mater. 126 (2009) 32–39.

Please cite this article as: C. Monticelli, et al., A study on the corrosion of reinforcing bars in alkali-activated fly ash mortars under wet and dry exposures to chloride solutions, Cem. Concr. Res. (2015), http://dx.doi.org/10.1016/j.cemconres.2016.05.010